



Mid-Course Assessment

# Hierarchically Modelling Stars Using Deep Learning and Asteroseismology

By

Alexander J. Lyttle

*Student ID* 1532473

*Supervisor* Dr Guy R. Davies

*Co-Supervisor* Dr Andrea Miglio

Solar and Stellar Physics Group  
School of Physics and Astronomy  
College of Engineering and Physical Sciences  
University of Birmingham

September 10, 2020

© Copyright by ALEXANDER J. LYTTLE, 2020

All Rights Reserved

## **ABSTRACT**

Your abstract goes here

## **ACKNOWLEDGMENTS**

I acknowledge the people who helped me.

# Contents

	Page
<b>1 Introduction</b>	<b>1</b>
1.1 Hierarchical Bayesian Models . . . . .	1
1.2 Modelling a Star . . . . .	6
1.3 Astroseismology . . . . .	6
1.3.1 Solar-like oscillators . . . . .	7
1.4 Sampling Stellar Models . . . . .	8
1.4.1 Grid-Based Modelling . . . . .	8
1.4.2 Neural Network . . . . .	8
1.5 Observing Stars . . . . .	8
1.5.1 Detecting Asteroseismic Oscillation Modes . . . . .	8
<b>2 Peakbagging with PBjam</b>	<b>9</b>
2.1 How it Works . . . . .	9
2.2 Contributing to the Code . . . . .	9
2.3 Peakbagging with TESS . . . . .	9
<b>3 Hierarchically Modelling Many Stars</b>	<b>10</b>
<b>4 Future Work</b>	<b>11</b>
4.1 Including the Helium II Glitch . . . . .	11
4.2 Increasing the Sample Size . . . . .	11

4.3 To Higher Mass Stars and Beyond . . . . .	11
<b>References</b>	<b>12</b>
<b>Appendix A Accompanying Paper</b>	<b>23</b>

# List of Figures

1.1	Luminosity against true ages of a fake stellar cluster. The true luminosities lie on the red line and the observed luminosities (black) have been artificially scattered by $0.05 L_{\odot}$ .	4
1.2	The $z$ -score, $(\bar{\tau} - \tau_{\text{true}})/s_{\tau}$ , where $\bar{\tau}$ and $s_{\tau}$ are the respective sample mean and standard deviation of the posterior ages from each of the no- and partially-pooled models.	5
1.3	Standard deviations, $s_{\tau}$ of the age posteriors from both the no- and partially-pooled models.	6

# List of Tables







# Chapter 1

## Introduction

### 1.1 Hierarchical Bayesian Models

Consider a model for a single object comprising a set of independent parameters,  $\boldsymbol{\theta} = \{\theta_i\}_{i=1}^{N_\theta}$  which makes a set of predictions,  $\boldsymbol{\mu}_y = \{\mu_{y,j}\}_{j=1}^{N_y}$  where  $\boldsymbol{\mu}_y = \mathbf{f}(\boldsymbol{\theta})$ . Using Bayes' theorem, we may write the *posterior* probability density function (PDF) of the model given a set of observations  $\mathbf{y}$  as,

$$p(\boldsymbol{\theta}|\mathbf{y}) = \frac{p(\mathbf{y}|\boldsymbol{\theta}) p(\boldsymbol{\theta})}{p(\mathbf{y})}, \quad (1.1)$$

where  $p(\mathbf{y}|\boldsymbol{\theta})$  is the *likelihood* of the data given the model,  $p(\boldsymbol{\theta})$  is the *a priori* PDF of the model parameters, and  $p(\mathbf{y})$  is the *evidence* of the data.

Assuming our observations of  $\mathbf{y}$  are uncorrelated and subjected to random, Gaussian noise with a known standard deviation,  $\sigma_y$ , we may write the likelihood function as a normal distribution,

$$p(\mathbf{y}|\boldsymbol{\theta}) = \prod_{j=1}^{N_y} \frac{1}{\sigma_{y,j} \sqrt{2\pi}} \exp \left[ -\frac{(y_j - \mu_{y,j})^2}{2\sigma_{y,j}^2} \right], \quad (1.2)$$

$$\equiv \prod_{j=1}^{N_y} \mathcal{N}(y_j | \mu_{y,j}, \sigma_{y,j}). \quad (1.3)$$

The prior PDF of the model, assuming the parameters are independent, is  $p(\boldsymbol{\theta}) = \prod_i p(\theta_i)$ . Encoding our prior understanding of the model this way is useful for improving our inference. For example, we have independent evidence that the age of the universe is  $\sim 14$  Gyr [CITE]. Hence, we may choose to give the age parameter for a stellar model a uniform prior PDF from 0 to 14 Gyr such that our posterior PDF is not influenced by unphysical ages.

The evidence is the PDF of the observational data. We write this as the normalisation of the numerator of Equation 1.1,

$$p(\mathbf{y}) = \int_{-\infty}^{+\infty} p(\mathbf{y}|\boldsymbol{\theta}) p(\boldsymbol{\theta}) d\boldsymbol{\theta}. \quad (1.4)$$

There are many ways to determine the posterior PDF, either analytically or numerically using e.g. Markov chain Monte Carlo (MCMC) through algorithms such as Metropolis-Hastings and Hamiltonian Monte-Carlo (HMC) [CITE]. Once we have the posterior, we can determine the marginalised posterior distribution of an individual parameter by integrating over all other parameters. For example, the marginalised posterior for  $\theta_1$  is,

$$p(\theta_1|\mathbf{y}) = \int_{-\infty}^{+\infty} p(\boldsymbol{\theta}|\mathbf{y}) d\theta_2 \dots d\theta_{N_\theta}. \quad (1.5)$$

Therefore, we end up with a distribution which describes the probability of  $\theta_1$  given  $\mathbf{y}$  which takes into account the distribution (or uncertainty) of all other parameters in the model.

The model described above can be applied to a single object such as a star. Let us now consider modelling a population of  $N_{\text{obj}}$  similar objects. We could combine the posteriors for each object to get a posterior for the population of objects,

$$p(\boldsymbol{\Theta}|\mathbf{Y}) = \prod_{k=1}^{N_{\text{obj}}} p(\boldsymbol{\theta}_k|\mathbf{y}_k), \quad (1.6)$$

where  $\boldsymbol{\Theta} = \{\boldsymbol{\theta}_k\}_{k=1}^{N_{\text{obj}}}$  and  $\mathbf{Y} = \{\mathbf{y}_k\}_{k=1}^{N_{\text{obj}}}$  are the matrices of model parameters and observations. We refer to this as a *no-pooled* model because no information is shared between the objects. However, what if we have a model which describes the distribution of a particular  $\theta_i$  in the population? For

example, if all the objects are stars in an open cluster which formed at roughly the same time, such as Messier 67 [CITE], we might want to encode such information into the model. One method would be to independently model the stars in the cluster and then find their population mean and standard deviation in age. It has been shown that this method typically over-predicts the standard deviation because it propagates the object-level uncertainties [CITE]. Alternatively, we can incorporate the assumption that stars in a cluster formed at the same time using one of two ways. The first is to *partially-pool* and the second is to *max-pool* the stellar ages respectively. The former assumes the object-level parameters are drawn from some common distribution, and the latter is the special case where all object-level parameters share the same value in the population.

We refer to models which pool parameters in this way as hierarchical models [CITE]. We describe the distribution of  $\Theta$  in the population by a set of *hyper-parameters*,  $\phi = \{\phi_l\}_{l=1}^{N_\phi}$ . Bayes' equation now becomes,

$$p(\phi, \Theta | Y) = \frac{p(Y | \Theta) p(\Theta | \phi) p(\phi)}{p(Y)} \quad (1.7)$$

where the probability of  $\Theta$  given  $\phi$  is,

$$p(\Theta | \phi) = \prod_{k=1}^{N_{\text{obj}}} d(\theta_k | \phi), \quad (1.8)$$

and  $d(\theta_k | \phi)$  is some chosen distribution from which the parameters for a given object are drawn from the population.

Let us consider a simple model which predicts the luminosities,  $L$  from the ages,  $\tau$  of  $N_{\text{obj}} = 1000$  stars in a cluster formed at roughly the same time. Modelling the population independently, we get the posterior,

$$p(\tau | L) \propto \prod_{k=1}^{1000} p(L_k | \tau_k) p(\tau_k). \quad (1.9)$$

Now, let us consider a partially-pooled model where the stellar ages are drawn from a normal distribution centred on a mean,  $\mu_\tau$  and standard deviation,  $\sigma_\tau$ . The posterior now becomes,

$$p(\mu_\tau, \sigma_\tau, \tau | L) \propto p(L | \tau) p(\tau | \mu_\tau, \sigma_\tau) p(\mu_\tau, \sigma_\tau), \quad (1.10)$$

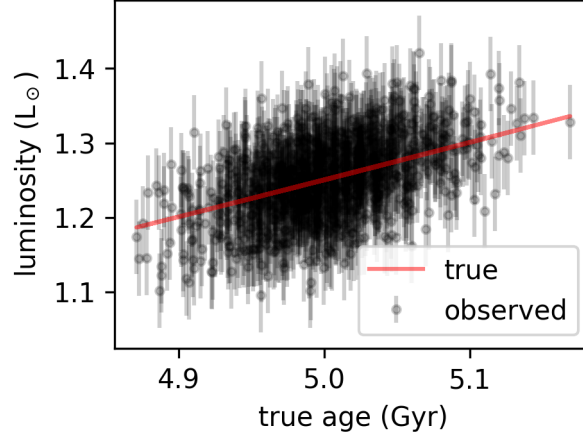


Figure 1.1: Luminosity against true ages of a fake stellar cluster. The true luminosities lie on the red line and the observed luminosities (black) have been artificially scattered by  $0.05 L_{\odot}$ .

where,

$$p(\boldsymbol{\tau}|\boldsymbol{\mu}_{\tau}, \boldsymbol{\sigma}_{\tau}) = \prod_{k=1}^{1000} \mathcal{N}(\tau_k|\boldsymbol{\mu}_{\tau}, \boldsymbol{\sigma}_{\tau}). \quad (1.11)$$

There is no known analytical or empirical relation between the age of a star and its luminosity, but for the purposes of this example let us say that we know  $L \propto \tau^2$ . I generated 1000 stellar ages from a normal distribution with a mean of 5 Gyr and a standard deviation of 0.05 Gyr, and computed their luminosities using this relation. Then, I added Gaussian noise to the luminosities with a standard deviation of  $0.05 L_{\odot}$  and proceeded to model the stellar ages using Equations 1.9 and 1.10 and the Bayesian package `pymc3` [CITE]. The observed and true luminosities are plot against the true ages in Figure 1.1 to show

If we wished to determine spread of stellar ages in the cluster using the no-pooled mode, we might naïvely calculate a standard deviation from the resulting stellar ages. However, this overestimates the true standard deviation, getting 0.109 Gyr rather than 0.05 Gyr, because it includes the uncertainty in the individual ages. When we model the population mean and spread in the hierarchical model we get  $\mu_{\tau} = 5.002 \pm 0.003$  Gyr and  $\sigma_{\tau} = 0.042 \pm 0.007$  Gyr which are within  $< 2\sigma$  of the truths. Therefore, the hierarachical model is a better way of determining population-

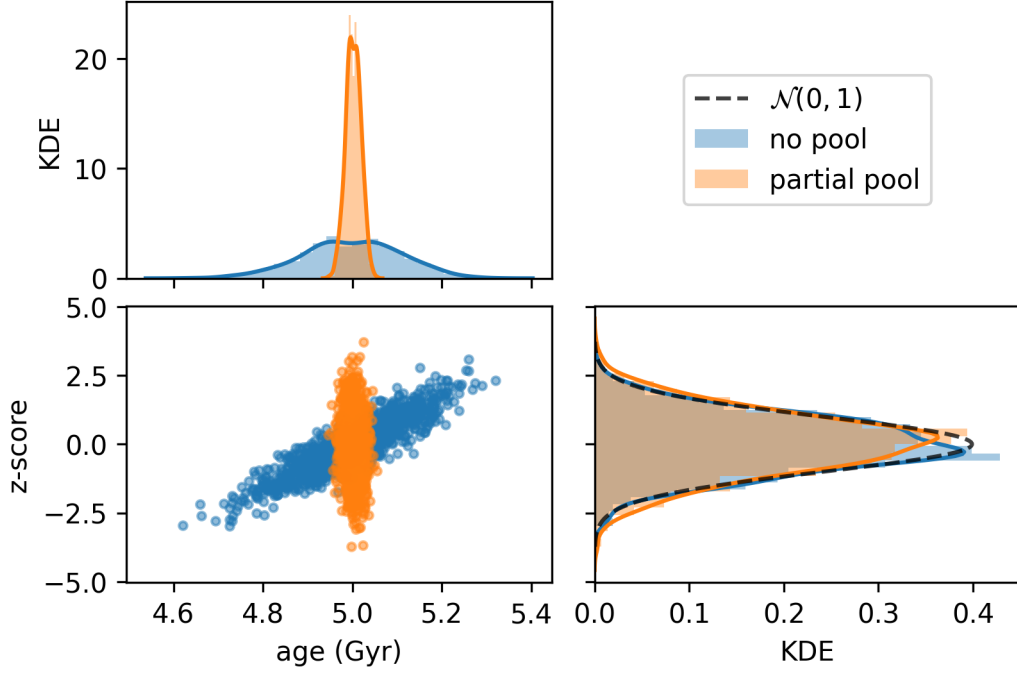


Figure 1.2: The  $z$ -score,  $(\bar{\tau} - \tau_{\text{true}})/s_{\tau}$ , where  $\bar{\tau}$  and  $s_{\tau}$  are the respective sample mean and standard deviation of the posterior ages from each of the no- and partially-pooled models.

level statistics than the traditional no-pooled model.

Both models can accurately determine ages, but the hierarchical model returns more precise ages, assuming our prior assumptions are true. Figure 1.2 shows that the  $z$ -score for ages from both models match a normal distribution with a mean of 0 and standard deviation of 1, indicating the individual stellar ages and uncertainties are accurate. However, the partially pooled model produces more than doubly precise ages, as shown in Figure 1.3, because the model takes into account the population mean and spread as hyper-parameters. The reduced scatter on stellar ages is also reflected in the top-left plot of Figure 1.2.

If we wish to improve the precision of fundamental stellar parameters, using hierarchical models to encode our prior knowledge is essential. However, modelling stars is not as simple, nor analytical as in the example above. Before we can statistically model a population of stars, we must

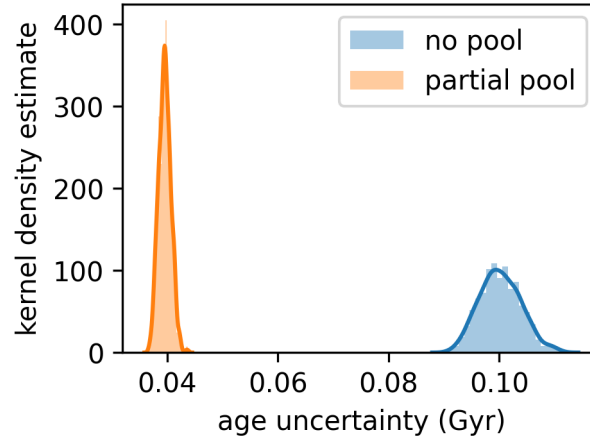


Figure 1.3: Standard deviations,  $s_\tau$  of the age posteriors from both the no- and partially-pooled models.

have a way of generating stellar observables from fundamental parameters such as age and mass. In the next section, I give an overview of how we numerically model stellar observables and why traditional methods pose new problems when adapting the above model.

## 1.2 Modelling a Star

Initial conditions mapping to observables. What is MESA.

## 1.3 Astroseismology

For over a century, we have been able to map stars based on their photometric magnitude and spectroscopic colour using Hertzsprung-Russell (HR) diagrams. Coupling such observational data with measurements of interstellar distances using parallax, we were able to determine stellar luminosities. The unique structure of early HR diagrams eluded to the idea that stars evolve over time. With the addition of nuclear physics, theories of stellar evolution could be put to the test.



However, while we could only observe stellar surface properties, many modelling mysteries would be left unsolved.

Until the last few decades, our understanding of stellar structure has been all but skin deep. In the 1960s, observations of 5-minute brightness fluctuations in the solar photosphere lead to the study of stochastically driven acoustic waves trapped beneath the surface of the Sun (Ulrich, 1970; Ando and Osaki, 1975). Later named helioseismology (Deubner and Gough, 1984), the study of oscillation modes allowed for further insights into the solar interior, such as rotation (Deubner, Ulrich, and Rhodes, 1979) and solar neutrino production (Bahcall and Ulrich, 1988). In tandem with this research was the emergence of asteroseismology – the study of stars through their oscillation frequencies (Christensen-Dalsgaard, 1984).

Give examples of the sorts of things asteroseismology can help us uncover, from ages (Ulrich, 1986; Soderblom, 2010; Silva Aguirre, Davies, et al., 2015, see, e.g.) to masses and radii from scaling relations () and fitting stellar models().

### **1.3.1 Solar-like oscillators**

Solar-like oscillators are stars for which their acoustic oscillator modes (or p modes) are excited stochastically by convection in their outer layers.

Review some work on solar-like oscillators and fundamental parameters.

## **1.4 Sampling Stellar Models**

### **1.4.1 Grid-Based Modelling**

### **1.4.2 Neural Network**

## **1.5 Observing Stars**

### **1.5.1 Detecting Asteroseismic Oscillation Modes**

Name some missions which were able to detect asteroseismic oscillations and review their limitations.

Explain the types of stars which can be observed and methods we can obtain the oscillations

## **Chapter 2**

# **Peakbagging with PBjam**

### **2.1 How it Works**

### **2.2 Contributing to the Code**

### **2.3 Peakbagging with TESS**

## **Chapter 3**

# **Hierarchically Modelling Many Stars**

See the accompanying paper (Appendix A).

# **Chapter 4**

## **Future Work**

### **4.1 Including the Helium II Glitch**

### **4.2 Increasing the Sample Size**

### **4.3 To Higher Mass Stars and Beyond**

Our next step is to include intermediate-mass stars with masses from approx. 1.2 solar masses to 3.0 solar masses.

# References

- Ahumada, Romina et al. (2019). “The Sixteenth Data Release of the Sloan Digital Sky Surveys: First Release from the APOGEE-2 Southern Survey and Full Release of eBOSS Spectra”. In: *arXiv e-prints* 1912, arXiv:1912.02905.
- Anderson, Lauren et al. (2018). “Improving Gaia Parallax Precision with a Data-Driven Model of Stars”. In: *AJ* 156, p. 145. doi: [10.3847/1538-3881/aad7bf](https://doi.org/10.3847/1538-3881/aad7bf).
- Ando, H. and Y. Osaki (1975). “Nonadiabatic Nonradial Oscillations - an Application to the Five-Minute Oscillation of the Sun”. In: *Publications of the Astronomical Society of Japan* 27, pp. 581–603.
- Asplund, Martin et al. (2009). “The Chemical Composition of the Sun”. In: *ARA&A* 47, pp. 481–522. doi: [10.1146/annurev.astro.46.060407.145222](https://doi.org/10.1146/annurev.astro.46.060407.145222).
- Astropy Collaboration, A. M. Price-Whelan, et al. (2018). “The Astropy Project: Building an Open-Science Project and Status of the v2.0 Core Package”. In: *AJ* 156, p. 123. doi: [10.3847/1538-3881/aabc4f](https://doi.org/10.3847/1538-3881/aabc4f).
- Astropy Collaboration, Thomas P. Robitaille, et al. (2013). “Astropy: A Community Python Package for Astronomy”. In: *A&A* 558, A33. doi: [10.1051/0004-6361/201322068](https://doi.org/10.1051/0004-6361/201322068).
- Bahcall, John N. and Roger K. Ulrich (1988). “Solar Models, Neutrino Experiments, and Helioseismology”. In: *Reviews of Modern Physics* 60, pp. 297–372. doi: [10.1103/RevModPhys.60.297](https://doi.org/10.1103/RevModPhys.60.297).

- Balser, Dana S. (2006). “The Chemical Evolution of Helium”. In: *AJ* 132, pp. 2326–2332. doi: [10.1086/508515](https://doi.org/10.1086/508515).
- Bellinger, E. P. et al. (2019). “Stellar Ages, Masses, and Radii from Asteroseismic Modeling Are Robust to Systematic Errors in Spectroscopy”. en. In: *A&A* 622, A130. doi: [10.1051/0004-6361/201834461](https://doi.org/10.1051/0004-6361/201834461).
- Berger, Travis A., Daniel Huber, Eric Gaidos, et al. (2018). “Revised Radii of *Kepler* Stars and Planets Using *Gaia* Data Release 2”. en. In: *ApJ* 866.2, p. 99. doi: [10.3847/1538-4357/aada83](https://doi.org/10.3847/1538-4357/aada83).
- Berger, Travis A., Daniel Huber, Jennifer L. van Saders, et al. (2020). “The *Gaia*–*Kepler* Stellar Properties Catalog I: Homogeneous Fundamental Properties for 186,000 *Kepler* Stars”. In: *arXiv e-prints* 2001, arXiv:2001.07737.
- Bossini, D. et al. (2019). “Age Determination for 269 *Gaia* DR2 Open Clusters”. en. In: *A&A* 623, A108. doi: [10.1051/0004-6361/201834693](https://doi.org/10.1051/0004-6361/201834693).
- Bovy, Jo et al. (2016). “On Galactic Density Modeling in the Presence of Dust Extinction”. In: *ApJ* 818, p. 130. doi: [10.3847/0004-637X/818/2/130](https://doi.org/10.3847/0004-637X/818/2/130).
- Brogaard, K. et al. (2012). “Age and Helium Content of the Open Cluster NGC 6791 from Multiple Eclipsing Binary Members. II. Age Dependencies and New Insights”. In: *Astronomy and Astrophysics* 543, A106. doi: [10.1051/0004-6361/201219196](https://doi.org/10.1051/0004-6361/201219196).
- Broomhall, A.-M. et al. (2011). “Solar-Cycle Variations of Large Frequency Separations of Acoustic Modes: Implications for Asteroseismology”. In: *MNRAS* 413, pp. 2978–2986. doi: [10.1111/j.1365-2966.2011.18375.x](https://doi.org/10.1111/j.1365-2966.2011.18375.x).
- Campante, T. L. et al. (2016). “Spin-Orbit Alignment of Exoplanet Systems: Ensemble Analysis Using Asteroseismology”. In: *ApJ* 819, p. 85. doi: [10.3847/0004-637X/819/1/85](https://doi.org/10.3847/0004-637X/819/1/85).
- Casagrande, Luca et al. (2007). “The Helium Abundance and  $\Delta Y/\Delta Z$  in Lower Main-Sequence Stars”. In: *MNRAS* 382, pp. 1516–1540. doi: [10.1111/j.1365-2966.2007.12512.x](https://doi.org/10.1111/j.1365-2966.2007.12512.x).
- Chan, Victor C. and Jo Bovy (2020). “The *Gaia* DR2 Parallax Zero-Point: Hierarchical Modelling of Red Clump Stars”. In: *MNRAS* 493, pp. 4367–4381. doi: [10.1093/mnras/staa571](https://doi.org/10.1093/mnras/staa571).

- Chiappini, C. et al. (2015). “Young [  $\alpha$  /Fe]-Enhanced Stars Discovered by CoRoT and APOGEE: What Is Their Origin?” en. In: *A&A* 576, p. L12. DOI: [10.1051/0004-6361/201525865](https://doi.org/10.1051/0004-6361/201525865).
- Chiosi, C. and F. M. Matteucci (1982). “The Helium to Heavy Element Enrichment Ratio, Delta Y/Delta Z”. In: *A&A* 105, pp. 140–148.
- Christensen-Dalsgaard, J. (1982). “Seismological Studies of the Sun and Other Stars”. In: *Advances in Space Research* 2, pp. 11–19. DOI: [10.1016/0273-1177\(82\)90250-2](https://doi.org/10.1016/0273-1177(82)90250-2).
- (1984). “What Will Asteroseismology Teach Us”. In: p. 11.
- Christensen-Dalsgaard, J. and D. O. Gough (1980). “Is the Sun Helium-Deficient”. In: *Nature* 288, pp. 544–547. DOI: [10.1038/288544a0](https://doi.org/10.1038/288544a0).
- Corsaro, E., J. De Ridder, and R. A. García (2015). “High-Precision Acoustic Helium Signatures in 18 Low-Mass Low-Luminosity Red Giants: Analysis from More than Four Years of *Kepler* Observations★”. en. In: *A&A* 578, A76. DOI: [10.1051/0004-6361/201525922](https://doi.org/10.1051/0004-6361/201525922).
- Das, Payel and Jason L. Sanders (2019). “MADE: A Spectroscopic Mass, Age, and Distance Estimator for Red Giant Stars with Bayesian Machine Learning”. en. In: *Mon. Not. R. Astron. Soc.* 484, p. 294. DOI: [10.1093/mnras/sty2776](https://doi.org/10.1093/mnras/sty2776).
- Davies, G. R., V. Silva Aguirre, et al. (2016). “Oscillation Frequencies for 35 *Kepler* Solar-Type Planet-Hosting Stars Using Bayesian Techniques and Machine Learning”. en. In: *MNRAS* 456.2, pp. 2183–2195. DOI: [10.1093/mnras/stv2593](https://doi.org/10.1093/mnras/stv2593).
- Davies, G. R., W. J. Chaplin, et al. (2015). “Asteroseismic Inference on Rotation, Gyrochronology and Planetary System Dynamics of 16 Cygni”. In: *Monthly Notices of the Royal Astronomical Society* 446, pp. 2959–2966. DOI: [10.1093/mnras/stu2331](https://doi.org/10.1093/mnras/stu2331).
- Davies, G. R. and A. Miglio (2016). “Asteroseismology of Red Giants: From Analysing Light Curves to Estimating Ages”. In: *Astronomische Nachrichten* 337, p. 774. DOI: [10.1002/asna.201612371](https://doi.org/10.1002/asna.201612371).
- Deubner, F.-L., R. K. Ulrich, and E. J. Rhodes Jr. (1979). “Solar P-Mode Oscillations as a Tracer of Radial Differential Rotation”. In: *Astronomy and Astrophysics* 72, pp. 177–185.



- Deubner, Franz-Ludwig and Douglas Gough (1984). “Helioseismology: Oscillations as a Diagnostic of the Solar Interior”. In: *Annual Review of Astronomy and Astrophysics* 22, pp. 593–619. DOI: [10.1146/annurev.aa.22.090184.003113](https://doi.org/10.1146/annurev.aa.22.090184.003113).
- Ferguson, Jason W. et al. (2005). “Low-Temperature Opacities”. In: *The Astrophysical Journal* 623, pp. 585–596. DOI: [10.1086/428642](https://doi.org/10.1086/428642).
- Foreman-Mackey, Daniel et al. (2013). “Emcee: The MCMC Hammer”. In: *Publications of the Astronomical Society of the Pacific* 125, p. 306. DOI: [10.1086/670067](https://doi.org/10.1086/670067).
- Frankel, Neige et al. (2020). “Keeping It Cool: Much Orbit Migration, yet Little Heating, in the Galactic Disk”. In: *arXiv e-prints* 2002, arXiv:2002.04622.
- Gaia Collaboration, A. G. A. Brown, et al. (2018). “Gaia Data Release 2. Summary of the Contents and Survey Properties”. In: *Astronomy and Astrophysics* 616, A1. DOI: [10.1051/0004-6361/201833051](https://doi.org/10.1051/0004-6361/201833051).
- Gaia Collaboration, T. Prusti, et al. (2016). “The Gaia Mission”. In: *A&A* 595, A1. DOI: [10.1051/0004-6361/201629272](https://doi.org/10.1051/0004-6361/201629272).
- Ginsburg, Adam et al. (2019). “Astroquery: An Astronomical Web-Querying Package in Python”. In: *AJ* 157, p. 98. DOI: [10.3847/1538-3881/aafc33](https://doi.org/10.3847/1538-3881/aafc33).
- Goupil, MarieJo (2019). “Seismic Probe of Transport Processes in Red Giants”. In: *ArXiv191009361 Astro-Ph*. arXiv: [1910.09361 \[astro-ph\]](https://arxiv.org/abs/1910.09361).
- Green, Gregory M. et al. (2019). “A 3D Dust Map Based on Gaia, Pan-STARRS 1, and 2MASS”. In: *ApJ* 887, p. 93. DOI: [10.3847/1538-4357/ab5362](https://doi.org/10.3847/1538-4357/ab5362).
- Grevesse, N. and A. J. Sauval (1998). “Standard Solar Composition”. In: *Space Sci. Rev.* 85, pp. 161–174. DOI: [10.1023/A:1005161325181](https://doi.org/10.1023/A:1005161325181).
- Hall, Oliver J. et al. (2019). “Testing Asteroseismology with Gaia DR2: Hierarchical Models of the Red Clump”. In: *MNRAS* 486, pp. 3569–3585. DOI: [10.1093/mnras/stz1092](https://doi.org/10.1093/mnras/stz1092).
- Hawkins, Keith et al. (2017). “Red Clump Stars and Gaia: Calibration of the Standard Candle Using a Hierarchical Probabilistic Model”. In: *MNRAS* 471, pp. 722–729. DOI: [10.1093/mnras/stx1655](https://doi.org/10.1093/mnras/stx1655).

- Hekker, S. et al. (2012). “Solar-like Oscillations in Red Giants Observed with Kepler: Influence of Increased Timespan on Global Oscillation Parameters”. In: *Astronomy and Astrophysics* 544, A90. DOI: [10.1051/0004-6361/201219328](https://doi.org/10.1051/0004-6361/201219328).
- Hendriks, L. and C. Aerts (2019). “Deep Learning Applied to the Asteroseismic Modeling of Stars with Coherent Oscillation Modes”. In: *PASP* 131, p. 108001. DOI: [10.1088/1538-3873/aaceec](https://doi.org/10.1088/1538-3873/aaceec).
- Hogg, David W. (2012). “Data Analysis Recipes: Probability Calculus for Inference”. In: *arXiv e-prints* 1205, arXiv:1205.4446.
- Hogg, David W., Jo Bovy, and Dustin Lang (2010). “Data Analysis Recipes: Fitting a Model to Data”. In: *arXiv e-prints* 1008, arXiv:1008.4686.
- Hogg, David W. and Daniel Foreman-Mackey (2018). “Data Analysis Recipes: Using Markov Chain Monte Carlo”. In: *ApJS* 236, p. 11. DOI: [10.3847/1538-4365/aab76e](https://doi.org/10.3847/1538-4365/aab76e).
- Hogg, David W., Adam D. Myers, and Jo Bovy (2010). “Inferring the Eccentricity Distribution”. In: *ApJ* 725, pp. 2166–2175. DOI: [10.1088/0004-637X/725/2/2166](https://doi.org/10.1088/0004-637X/725/2/2166).
- Hon, Marc, Dennis Stello, and Jie Yu (2017). “Deep Learning Classification in Asteroseismology”. en. In: *Mon. Not. R. Astron. Soc.* 469.4, pp. 4578–4583. DOI: [10.1093/mnras/stx1174](https://doi.org/10.1093/mnras/stx1174).
- Hon, Marc, Dennis Stello, and Joel C. Zinn (2018). “Detecting Solar-like Oscillations in Red Giants with Deep Learning”. en. In: *ApJ* 859.1, p. 64. DOI: [10.3847/1538-4357/aabfdb](https://doi.org/10.3847/1538-4357/aabfdb).
- Howe, Rachel et al. (2020). “Solar Cycle Variation of  $N_{\max}$  in Helioseismic Data and Its Implications for Asteroseismology”. In: *MNRAS* 493, pp. L49–L53. DOI: [10.1093/mnras/slaa006](https://doi.org/10.1093/mnras/slaa006).
- Huber, D., T. R. Bedding, et al. (2011). “Testing Scaling Relations for Solar-like Oscillations from the Main Sequence to Red Giants Using Kepler Data”. In: *ApJ* 743, p. 143. DOI: [10.1088/0004-637X/743/2/143](https://doi.org/10.1088/0004-637X/743/2/143).
- Huber, D., D. Stello, et al. (2009). “Automated Extraction of Oscillation Parameters for Kepler Observations of Solar-Type Stars”. In: *Communications in Asteroseismology* 160, p. 74.
- Kahn, F. D. (1961). “Sound Waves Trapped in the Solar Atmosphere.” In: *The Astrophysical Journal* 134, p. 343. DOI: [10.1086/147164](https://doi.org/10.1086/147164).

- Kinemuchi, K. et al. (2012). “Demystifying Kepler Data: A Primer for Systematic Artifact Mitigation”. In: *Publications of the Astronomical Society of the Pacific* 124, p. 963. DOI: [10.1086/667603](https://doi.org/10.1086/667603).
- Kjeldsen, H. and T. R. Bedding (1995). “Amplitudes of Stellar Oscillations: The Implications for Asteroseismology.” In: *Astronomy and Astrophysics* 293, pp. 87–106.
- Kuszlewicz, James S. et al. (2019). “Bayesian Hierarchical Inference of Asteroseismic Inclination Angles”. In: *MNRAS* 488, pp. 572–589. DOI: [10.1093/mnras/stz1689](https://doi.org/10.1093/mnras/stz1689).
- Lebreton, Y., M.J. Goupil, and J. Montalbán (2014). “How Accurate Are Stellar Ages Based on Stellar Models?: I. The Impact of Stellar Models Uncertainties”. en. In: *EAS Publications Series* 65. Ed. by Y. Lebreton, D. Valls-Gabaud, and C. Charbonnel, pp. 99–176. DOI: [10.1051/eas/1465004](https://doi.org/10.1051/eas/1465004).
- Leistedt, Boris and David W. Hogg (2017). “Hierarchical Probabilistic Inference of the Color-Magnitude Diagram and Shrinkage of Stellar Distance Uncertainties”. In: *AJ* 154, p. 222. DOI: [10.3847/1538-3881/aa91d5](https://doi.org/10.3847/1538-3881/aa91d5).
- Licquia, Timothy C. and Jeffrey A. Newman (2015). “Improved Estimates of the Milky Way’s Stellar Mass and Star Formation Rate from Hierarchical Bayesian Meta-Analysis”. In: *ApJ* 806, p. 96. DOI: [10.1088/0004-637X/806/1/96](https://doi.org/10.1088/0004-637X/806/1/96).
- Lightkurve Collaboration et al. (2018). “Lightkurve: Kepler and TESS Time Series Analysis in Python”. In: *Astrophysics Source Code Library*, ascl:1812.013.
- Lindgren, L. et al. (2018). “Gaia Data Release 2. The Astrometric Solution”. In: *A&A* 616, A2. DOI: [10.1051/0004-6361/201832727](https://doi.org/10.1051/0004-6361/201832727).
- Lomb, N. R. (1976). “Least-Squares Frequency Analysis of Unequally Spaced Data”. In: *Astrophysics and Space Science* 39, pp. 447–462. DOI: [10.1007/BF00648343](https://doi.org/10.1007/BF00648343).
- Magic, Z., A. Weiss, and M. Asplund (2015). “The Stagger-Grid: A Grid of 3D Stellar Atmosphere Models. III. The Relation to Mixing Length Convection Theory”. In: *A&A* 573, A89. DOI: [10.1051/0004-6361/201423760](https://doi.org/10.1051/0004-6361/201423760).

- Martinez, Gregory D. (2015). “A Robust Determination of Milky Way Satellite Properties Using Hierarchical Mass Modelling”. In: *MNRAS* 451, pp. 2524–2535. DOI: [10.1093/mnras/stv942](https://doi.org/10.1093/mnras/stv942).
- Morton, Timothy D. (2015). “Isochrones: Stellar Model Grid Package”. In: *Astrophys. Source Code Libr.* ascl:1503.010.
- Morton, Timothy D. and Joshua N. Winn (2014). “Obliquities of Kepler Stars: Comparison of Single- and Multiple-Transit Systems”. In: *ApJ* 796, p. 47. DOI: [10.1088/0004-637X/796/1/47](https://doi.org/10.1088/0004-637X/796/1/47).
- Mosser, B. et al. (2015). “Period Spacings in Red Giants. I. Disentangling Rotation and Revealing Core Structure Discontinuities”. In: *Astronomy and Astrophysics* 584, A50. DOI: [10.1051/0004-6361/201527075](https://doi.org/10.1051/0004-6361/201527075).
- Nissen, P. E. et al. (2017). “High-Precision Abundances of Elements in Kepler LEGACY Stars. Verification of Trends with Stellar Age”. In: *Astronomy and Astrophysics* 608, A112. DOI: [10.1051/0004-6361/201731845](https://doi.org/10.1051/0004-6361/201731845).
- Ohn, Ilsang and Yongdai Kim (2019). “Smooth Function Approximation by Deep Neural Networks with General Activation Functions”. In: *Entropy* 21.7, p. 627. DOI: [10.3390/e21070627](https://doi.org/10.3390/e21070627). arXiv: [1906.06903](https://arxiv.org/abs/1906.06903).
- Paxton, Bill, Lars Bildsten, et al. (2011). “Modules for Experiments in Stellar Astrophysics (MESA)”. In: *ApJS* 192, p. 3. DOI: [10.1088/0067-0049/192/1/3](https://doi.org/10.1088/0067-0049/192/1/3).
- Paxton, Bill, Matteo Cantiello, et al. (2013). “Modules for Experiments in Stellar Astrophysics (MESA): Planets, Oscillations, Rotation, and Massive Stars”. In: *The Astrophysical Journal Supplement Series* 208, p. 4. DOI: [10.1088/0067-0049/208/1/4](https://doi.org/10.1088/0067-0049/208/1/4).
- Paxton, Bill, Pablo Marchant, et al. (2015). “Modules for Experiments in Stellar Astrophysics (MESA): Binaries, Pulsations, and Explosions”. In: *The Astrophysical Journal Supplement Series* 220, p. 15. DOI: [10.1088/0067-0049/220/1/15](https://doi.org/10.1088/0067-0049/220/1/15).
- Paxton, Bill, Josiah Schwab, et al. (2018). “Modules for Experiments in Stellar Astrophysics (MESA): Convective Boundaries, Element Diffusion, and Massive Star Explosions”. In: *The Astrophysical Journal Supplement Series* 234, p. 34. DOI: [10.3847/1538-4365/aaa5a8](https://doi.org/10.3847/1538-4365/aaa5a8).

- Paxton, Bill, R. Smolec, et al. (2019). “Modules for Experiments in Stellar Astrophysics (MESA): Pulsating Variable Stars, Rotation, Convective Boundaries, and Energy Conservation”. In: *The Astrophysical Journal Supplement Series* 243, p. 10. DOI: [10.3847/1538-4365/ab2241](https://doi.org/10.3847/1538-4365/ab2241).
- Pinsonneault, Marc H. et al. (2012). “A Revised Effective Temperature Scale for the Kepler Input Catalog”. In: *ApJS* 199, p. 30. DOI: [10.1088/0067-0049/199/2/30](https://doi.org/10.1088/0067-0049/199/2/30).
- Ramachandran, Prajit, Barret Zoph, and Quoc V. Le (2017). “Searching for Activation Functions”. In: *arXiv e-prints* 1710, arXiv:1710.05941.
- Reese, D. R. et al. (2016). “SpaceInn Hare-and-Hounds Exercise: Estimation of Stellar Properties Using Space-Based Asteroseismic Data”. In: *A&A* 592, A14. DOI: [10.1051/0004-6361/201527987](https://doi.org/10.1051/0004-6361/201527987).
- Ribas, Ignasi et al. (2000). “Chemical Composition of Eclipsing Binaries: A New Approach to the Helium-to-Metal Enrichment Ratio”. In: *MNRAS* 313, pp. 99–111. DOI: [10.1046/j.1365-8711.2000.03195.x](https://doi.org/10.1046/j.1365-8711.2000.03195.x).
- Rogers, F. J. and A. Nayfonov (2002). “Updated and Expanded OPAL Equation-of-State Tables: Implications for Helioseismology”. In: *The Astrophysical Journal* 576, pp. 1064–1074. DOI: [10.1086/341894](https://doi.org/10.1086/341894).
- Rogers, Leslie A. (2015). “Most 1.6 Earth-Radius Planets Are Not Rocky”. In: *ApJ* 801, p. 41. DOI: [10.1088/0004-637X/801/1/41](https://doi.org/10.1088/0004-637X/801/1/41).
- Salvatier, John, Thomas V. Wiecki, and Christopher Fonnesbeck (2016). “Probabilistic Programming in Python Using PyMC3”. en. In: *PeerJ Comput. Sci.* 2, e55. DOI: [10.7717/peerj-cs.55](https://doi.org/10.7717/peerj-cs.55).
- Sandquist, Eric L. et al. (2020). “Variability in the Massive Open Cluster NGC 1817 from K2: A Rich Population of Asteroseismic Red Clump, Eclipsing Binary, and Main Sequence Pulsating Stars”. In: *ArXiv200101839 Astro-Ph*. arXiv: [2001.01839 \[astro-ph\]](https://arxiv.org/abs/2001.01839).
- Scargle, J. D. (1982). “Studies in Astronomical Time Series Analysis. II - Statistical Aspects of Spectral Analysis of Unevenly Spaced Data”. In: *The Astrophysical Journal* 263, pp. 835–853. DOI: [10.1086/160554](https://doi.org/10.1086/160554).

- Serenelli, Aldo M. and Sarbani Basu (2010). “Determining the Initial Helium Abundance of the Sun”. In: *ApJ* 719, pp. 865–872. DOI: [10.1088/0004-637X/719/1/865](https://doi.org/10.1088/0004-637X/719/1/865).
- Serenelli, Aldo, Jennifer Johnson, et al. (2017). “The First APOKASC Catalog of Kepler Dwarf and Subgiant Stars”. In: *ApJS* 233, p. 23. DOI: [10.3847/1538-4365/aa97df](https://doi.org/10.3847/1538-4365/aa97df).
- Si, Shijing et al. (2017). “A Hierarchical Model for the Ages of Galactic Halo White Dwarfs”. In: *MNRAS* 468, pp. 4374–4388. DOI: [10.1093/mnras/stx765](https://doi.org/10.1093/mnras/stx765).
- Silva Aguirre, V., G. R. Davies, et al. (2015). “Ages and Fundamental Properties of Kepler Exoplanet Host Stars from Asteroseismology”. en. In: *MNRAS* 452.2, p. 2127. DOI: [10.1093/mnras/stv1388](https://doi.org/10.1093/mnras/stv1388).
- Silva Aguirre, Víctor, Mikkel N. Lund, et al. (2017). “Standing on the Shoulders of Dwarfs: The Kepler Asteroseismic LEGACY Sample. II. Radii, Masses, and Ages”. In: *ApJ* 835, p. 173. DOI: [10.3847/1538-4357/835/2/173](https://doi.org/10.3847/1538-4357/835/2/173).
- Smith, Jeffrey C. et al. (2012). “Kepler Presearch Data Conditioning II - A Bayesian Approach to Systematic Error Correction”. In: *Publications of the Astronomical Society of the Pacific* 124, p. 1000. DOI: [10.1086/667697](https://doi.org/10.1086/667697).
- Soderblom, David R. (2010). “The Ages of Stars”. en. In: *ARA&A* 48.1, pp. 581–629. DOI: [10.1146/annurev-astro-081309-130806](https://doi.org/10.1146/annurev-astro-081309-130806).
- Soni, Harsh et al. (2020). “Phases and Excitations of Active Rod-Bead Mixtures: Simulations and Experiments”. In: *ArXiv200100173 Cond-Mat*. arXiv: [2001.00173 \[cond-mat\]](https://arxiv.org/abs/2001.00173).
- Stumpe, Martin C. et al. (2012). “Kepler Presearch Data Conditioning I—Architecture and Algorithms for Error Correction in Kepler Light Curves”. In: *Publications of the Astronomical Society of the Pacific* 124, p. 985. DOI: [10.1086/667698](https://doi.org/10.1086/667698).
- Townsend, R. H. D. and S. A. Teitler (2013). “GYRE: An Open-Source Stellar Oscillation Code Based on a New Magnus Multiple Shooting Scheme”. In: *Monthly Notices of the Royal Astronomical Society* 435, pp. 3406–3418. DOI: [10.1093/mnras/stt1533](https://doi.org/10.1093/mnras/stt1533).

- Trampedach, Regner et al. (2014). “Improvements to Stellar Structure Models, Based on a Grid of 3D Convection Simulations - II. Calibrating the Mixing-Length Formulation”. In: *MNRAS* 445, pp. 4366–4384. DOI: [10.1093/mnras/stu2084](https://doi.org/10.1093/mnras/stu2084).
- Ulrich, R. K. (1986). “Determination of Stellar Ages from Asteroseismology”. In: *The Astrophysical Journal Letters* 306, pp. L37–L40. DOI: [10.1086/184700](https://doi.org/10.1086/184700).
- Ulrich, Roger K. (1970). “The Five-Minute Oscillations on the Solar Surface”. In: *The Astrophysical Journal* 162, p. 993. DOI: [10.1086/150731](https://doi.org/10.1086/150731).
- VanderPlas, Jacob T. (2018). “Understanding the Lomb-Scargle Periodogram”. In: *The Astrophysical Journal Supplement Series* 236, p. 16. DOI: [10.3847/1538-4365/aab766](https://doi.org/10.3847/1538-4365/aab766).
- Verma, Kuldeep, Shravan Hanasoge, et al. (2016). “Asteroseismic Determination of Fundamental Parameters of Sun-like Stars Using Multilayered Neural Networks”. In: *MNRAS* 461, pp. 4206–4214. DOI: [10.1093/mnras/stw1621](https://doi.org/10.1093/mnras/stw1621).
- Verma, Kuldeep, Keyuri Raodeo, et al. (2019). “Helium Abundance in a Sample of Cool Stars: Measurements from Asteroseismology”. In: *MNRAS* 483, pp. 4678–4694. DOI: [10.1093/mnras/sty3374](https://doi.org/10.1093/mnras/sty3374).
- Viani, Lucas S. et al. (2018). “Investigating the Metallicity-Mixing-Length Relation”. In: *The Astrophysical Journal* 858, p. 28. DOI: [10.3847/1538-4357/aab7eb](https://doi.org/10.3847/1538-4357/aab7eb).
- von Hippel, Ted et al. (2006). “Inverting Color-Magnitude Diagrams to Access Precise Star Cluster Parameters: A Bayesian Approach”. In: *ApJ* 645.2, pp. 1436–1447. DOI: [10.1086/504369](https://doi.org/10.1086/504369).
- Vrard, M. et al. (2015). “Helium Signature in Red Giant Oscillation Patterns Observed by *Kepler*”. In: *A&A* 579, A84. DOI: [10.1051/0004-6361/201425064](https://doi.org/10.1051/0004-6361/201425064).
- White, Timothy R. et al. (2011). “Calculating Asteroseismic Diagrams for Solar-like Oscillations”. In: *The Astrophysical Journal* 743, p. 161. DOI: [10.1088/0004-637X/743/2/161](https://doi.org/10.1088/0004-637X/743/2/161).
- Zinn, Joel C., Marc H. Pinsonneault, Daniel Huber, and Dennis Stello (2019). “Confirmation of the Gaia DR2 Parallax Zero-Point Offset Using Asteroseismology and Spectroscopy in the *Kepler* Field”. In: *ApJ* 878, p. 136. DOI: [10.3847/1538-4357/ab1f66](https://doi.org/10.3847/1538-4357/ab1f66).

Zinn, Joel C., Marc H. Pinsonneault, Daniel Huber, Dennis Stello, et al. (2019). “Testing the Radius Scaling Relation with Gaia DR2 in the Kepler Field”. In: *ApJ* 885, p. 166. doi: [10.3847/1538-4357/ab44a9](https://doi.org/10.3847/1538-4357/ab44a9).



# **Appendix A**

## **Accompanying Paper**

# TBC: Hierarchically modelling *Kepler* dwarfs using machine learning to uncover helium enrichment in the solar neighbourhood

Alexander J. Lyttle,<sup>1,2</sup>★ Tanda Li,<sup>1,2</sup> Guy R. Davies,<sup>1,2</sup> Lindsey M. Carboneau<sup>1,2</sup> and TBC

<sup>1</sup>*School of Physics and Astronomy, University of Birmingham, Birmingham, B15 2TT, UK*

<sup>2</sup>*Stellar Astrophysics Centre (SAC), Department of Physics and Astronomy, Aarhus University, Ny Munkegade 120, DK-8000 Aarhus C, Denmark*

Accepted XXX. Received YYY; in original form ZZZ

## ABSTRACT

### Key words:

asteroseismology – methods: miscellaneous – methods: statistical – stars: fundamental parameters – stars: low-mass

## 1 INTRODUCTION

Motivation - precise and accurate stellar fundamentals. Useful for e.g. galactic archaeology and exoplanet research.

Audience - astrophysicist with some knowledge Introduce new method and reference Guy’s paper:

- Summarise the typical way in which stellar fundamentals are estimated and their pitfalls (e.g. discrete sampling, and assuming solar calibrated mixing-length parameter and helium enrichment)
  - Problems with grid-based-modelling (e.g. proper sampling)
  - assuming fixed DYDZ and MLT bad; attempts to interpolate, slow and hard to scale
- Why hierarchical models are good with examples of HBMs in astrophysics
  - Advantage of HBM is to incorporate population-level distributions
  - Why HBMs are difficult with stellar models.
  - Introduce the neural network as a way to overcome these issues and give examples of neural networks to approximate models in astrophysics
  - Highlight the novel element of this paper - the first application of combining a neural network emulator with a hierarchical model to provide shrinkage of fundamentals uncertainties and simultaneously study a helium enrichment relation
  - Use a helium enrichment law prior, and assume a distribution of mixing-length of the population-level, to inform object-level parameters

Why do we care about helium and mixing-length? These parameters have a large (be quantitative) affect on stellar ages. Good stellar ages allow us to better study galactic archaeology (with citations).

Given that we are assuming a helium enrichment prior, give a

brief summary of research into the helium enrichment and typical values for  $\Delta Y/\Delta Z$ . Note that in reality there may not be a linear law, and more may be studied in future work (or using a GP like in Guy’s paper?). Why do we care about an enrichment law? Why is it physically justified?

Given that we are assuming a mixing-length distribution, mention this is mainly a nuisance parameter which we will marginalize over, since this differs depending on model physics. However, later justify a normal spread by referring to work (e.g. Magic) which shows little variation in the area of the HRD we are studying.

Outline the structure of the work. We are demonstrating the method on an asteroseismic sample of dwarfs and subgiants from Serenelli 2017. We first introduce the data and why we choose to use spectroscopy and asteroseismology. We then introduce the method, from the grid of stellar models

Why asteroseismology and why this particular set of *Kepler*-field dwarfs? Acknowledge selection bias but explain that with TESS providing an all-sky sample of solar-like oscillators this method can be extended to a much larger sample size.

Note: here is an example of a paper which would benefit from a value of the intrinsic spread in helium enrichment: (Zinn et al. 2019) ‘Until such a time as the intrinsic scatter in helium enrichment can be determined, which... hinders a comparison between the theoretical metallicity trend and the observed radius agreement... the asteroseismic scaling relation radius does not require a metallicity term...’. In other words, they assume a helium enrichment law but this hinders their ability to study the seismic scaling relation correction.

## 2 DATA

We began with the sample of 415 stars from the first APOKASC catalogue of dwarfs and subgiants (S17). It is, to date, the most comprehensive sample of asteroseismic dwarfs and subgiant stars observed by the *Kepler* mission. We adopted the global asteroseismic parameters – the large frequency separation,  $\Delta\nu$ , and the

★ E-mail: ajl573@student.bham.ac.uk

frequency of maximum power,  $\nu_{\max}$  – determined by S17, and references therein. We then cross matched the sample with *Gaia* Data Release 2 for high-precision parallaxes and the Apache Point Observatory Galaxy Evolution Experiment (APOGEE) catalogue to obtain spectroscopic metallicities and effective temperatures. Using the cross matched catalogue, we calculated luminosities for the full sample with Two-Micron All Sky Survey (2MASS) photometry and selected a subsample of stars with similar metallicities and masses. Our method is described in detail in the remainder of this section.

We cross matched the *Kepler* input catalogue (KIC) for the sample with the *Gaia* DR2 catalogue taking the nearest neighbours within a 4" radius [CITE GAIA]. All but two of the sample of 415 stars were available. We then adopted the *Gaia* parallaxes, assuming a zero-point offset of 0.05 mas in the sense that the *Gaia* parallaxes are underestimated. We chose this value in line with recent studies on the *Gaia* zero-point parallax offset in the *Kepler* field [CITATIONS].

We adopted spectroscopic metallicities,  $[M/H]$ , and effective temperatures,  $T_{\text{eff}}$  determined by the APOGEE stellar parameters and chemical abundances pipeline (ASPCAP) from the second data release of the fourth phase of the Sloan Digital Sky Survey (SDSS) otherwise known as Data Release 14 (DR14). We cross matched the APOGEE DR14 catalogue with our *Kepler-Gaia* DR2 cross match yielding spectroscopic parameters for all 413 stars in the sample.

In order to remove more evolved stars, we made a cut in surface gravity,  $g$ . We used asteroseismic  $\nu_{\max}$  with ASPCAP  $T_{\text{eff}}$  and rearranged the asteroseismic scaling relation to get,

$$\log g \approx \log g_{\odot} + \log \left( \frac{\nu_{\max}}{\nu_{\max,\odot}} \right) - \frac{1}{2} \log \left( \frac{T_{\text{eff}}}{T_{\text{eff},\odot}} \right), \quad (1)$$

where solar reference values of  $\nu_{\max,\odot} = 3090 \pm 30 \mu\text{Hz}$  (Huber et al. 2011)  $\log g_{\odot} = 4.44$  dex and  $T_{\text{eff},\odot} = 5777$  K were used to determine the log surface gravity,  $\log g$ .

We determined luminosities for the sample using the direct method of ISOCCLASSIFY [CITE HUBER]. We calculated absolute  $K_s$ -band magnitudes using  $K_s$ -band photometry from the 2MASS, distances from the zero-point-offset-corrected parallaxes from *Gaia* DR2 and extinctions determined from the 3D galactic reddening maps of Green et al. (2019) [CITE]. We then determined absolute bolometric magnitudes by interpolating the MIST bolometric correction tables using ASPCAP  $[M/H]$  and  $T_{\text{eff}}$ , asteroseismic  $\log g$  and absolute magnitude as inputs. An uncertainty of 0.02 mag was assumed for both the extinctions and bolometric corrections, in line with typical uncertainties from randomly sampling the input data within their errors. The resulting distances, absolute magnitudes and luminosities with their respective uncertainties are given in Table X.

We selected a subset from the above sample which we determined to lie within the bounds of the model grid described in Section 3.1 using mass estimates from S17. We determined such “on-grid” stars where their estimated mass and metallicity were within one standard deviation of the grid boundary, from 0.8 to 1.2  $M_{\odot}$  in mass and from  $-0.5$  to  $0.5$  dex in metallicity. We also cut targets in the sample with an asteroseismic  $\log g$  less than 3.8 dex to remove more evolved stars. The cut in mass was motivated by our choice of model physics described in Section 3.1. Stars with  $M \gtrsim 1.15 M_{\odot}$  are understood to have a convective, hydrogen-burning core, with some dependence on the choice of stellar physics [CITE Appourchaux]. Modelling stars with a convective core requires the consideration of extra mixing due to the overshooting of convective cells at the

core boundary [CITE OVERSHOOT PAPERS], which is beyond the scope of this work.

The final sample comprised 81 stars, after removing stars with null observables. The data for 10 stars from the sample is shown in Table 1 and the full table may be downloaded LINK. The Hertzsprung-Russell diagram in Figure ?? shows the sample plot above a selection of stellar evolutionary tracks from the grid described in Section 3.1. A second plot shows the sample in context with a selection of *Kepler* solar neighbourhood stars. Consider the range of parallaxes plot when defining the solar neighbourhood (less than 1 kpc).

### 3 METHODS

Outline the model and its requirements with justification before introducing the following subsections.

#### 3.1 Grid of stellar models

We built up a stellar model grid to train the NN model. The grid includes four independent model inputs: stellar mass ( $M$ ), initial helium fraction ( $Y_{\text{init}}$ ), initial metallicity ( $[Fe/H]$ ), and the mixing-length parameter ( $\alpha_{\text{MLT}}$ ). Ranges and grid steps of the four model inputs are summarised in Table 2. We computed each stellar evolutionary track from the Hayashi line and to the base of red-giant branch where  $\log g = 3.6$  dex. We also computed 4,000 evolutionary tracks with random input values in the parameter space for validating the results.

##### 3.1.1 Stellar models and input physics

We used Modules for Experiments in Stellar Astrophysics (MESA, version 12115) to establish a grid of stellar models. MESA is an open-source stellar evolution package which is undergoing active development. Descriptions of input physics and numerical methods can be found in Paxton et al. (2011, 2013, 2015). We adopted the solar chemical mixture  $[(Z/X)_{\odot} = 0.0181]$  provided by Asplund et al. (2009). The initial chemical composition was calculated by:

$$\log(Z_{\text{init}}/X_{\text{init}}) = \log(Z/X)_{\odot} + [Fe/H]. \quad (2)$$

We used the MESA  $\rho - T$  tables based on the 2005 update of OPAL EOS tables (Rogers & Nayfonov 2002) and OPAL opacity supplemented by low-temperature opacity (Ferguson et al. 2005). The MESA ‘simple’ photosphere were used as the set of boundary conditions for modelling the atmosphere. The mixing-length theory of convection was implemented, where  $\alpha_{\text{MLT}} = \ell_{\text{MLT}}/H_p$  is the mixing-length parameter. We also applied the MESA predictive mixing scheme (Paxton et al. 2018, 2019) in the model computation.

The evolution time step was mainly controlled by the set-up tolerances on changes in surface effective temperature and luminosity. We saved one structural model at every time step at main sequence and every two steps after central hydrogen exhaustion. For each evolutionary track, we obtained  $\sim 100$  at the main-sequence stage and 500 – 700 at evolved stages.

##### 3.1.2 Oscillation models and seismic $\Delta\nu$

Theoretical stellar oscillations were calculated with the GYRE code (version 5.1), which was developed by Townsend & Teitler (2013). And we computed radial modes (for  $\ell = 0$ ) by solving the adiabatic stellar pulsation equations with the structural models generated by

Table 1.

Name	$T_{\text{eff}}$ (K)	$\sigma T_{\text{eff}}$ (K)	$L$ ( $L_{\odot}$ )	$\sigma L$ ( $L_{\odot}$ )	$\Delta\nu$ ( $\mu\text{Hz}$ )	$\sigma_{\Delta\nu}$ ( $\mu\text{Hz}$ )	[M/H] (dex)	$\sigma_{[\text{M}/\text{H}]}$ (dex)	$\log g$ (dex)	$\sigma_{\log g}$ (dex)
KIC10079226	5928.84	124.84	1.57	0.05	116.04	0.73	0.16	0.07	4.36	0.01
KIC10215584	5666.92	119.33	1.64	0.06	115.16	2.83	0.04	0.07	4.27	0.09
KIC10319352	5456.17	106.65	1.85	0.06	78.75	1.73	0.27	0.06	3.96	0.13
KIC10322381	6146.79	148.58	2.44	0.08	86.64	6.57	-0.32	0.08	4.19	0.04
KIC10417911	5628.26	109.99	3.41	0.12	56.14	2.10	0.34	0.07	3.94	0.02
KIC10732098	5669.65	119.28	3.02	0.12	62.18	1.92	0.05	0.07	3.96	0.02
KIC10794845	6035.12	140.46	1.64	0.06	116.35	6.70	-0.21	0.08	4.40	0.11
KIC10963065	6039.78	139.10	1.88	0.06	103.21	0.11	-0.16	0.08	4.30	0.01
KIC10971974	5748.00	142.40	1.43	0.05	106.63	3.31	-0.07	0.09	4.32	0.04
KIC11021413	5329.18	102.98	3.16	0.11	48.16	1.29	0.01	0.04	3.84	0.01

Table 2. Stellar model computations for training and test datasets.

Training model set (Grid-based)			
Input Parameter	Range	Increment	$N_{\text{train}}$
$M$ [ $M_{\odot}$ ]	0.80 – 1.20	0.01	15,375
[Fe/H] [dex]	-0.5 – 0.2/0.2 – 0.5	0.1/0.05	
$Y_{\text{init}}$	0.24 – 0.32	0.02	
$\alpha_{\text{MLT}}$	1.7 – 2.5	0.2	

MESA. We computed a seismic large separation ( $\Delta\nu$ ) for each model with theoretical radial modes to avoid the systematic offset of the scaling relation. We derived  $\Delta\nu$  with the approach given by White et al. (2011), which is a weighted least-squares fit to the radial frequencies as a function of  $n$ .

### 3.2 Artificial neural network

**Artificial neural network (ANN).** Introduce, with reference, the principle behind a neural network and the way in which it can be evaluated. Used Tensorflow etc. The following will work much better in a diagram.

- Initial mass,  $M$
- Initial helium fraction,  $Y_{\text{init}}$
- Initial metals fraction,  $Z_{\text{init}}$
- Mixing-length-theory parameter,  $\alpha_{\text{mlt}}$
- Fractional main-sequence lifetime,  $f_{\text{MS}}$

The training dataset comprised the inputs and outputs of the grid of stellar models described in Section 3.1. We chose the ANN inputs to correspond to the following model fundamentals... with the exception of age, which serves best as an output for the following reason. Age is understood to scale with at least mass and fractional main-sequence lifetime (citation). We found that the ANN performed better with a proxy for age as input, and age as an output.

We chose the ANN outputs to correspond to, or allow derivation of, observables,

- Effective temperature,  $T_{\text{eff}}$
- Radius,  $R$
- Large frequency separation,  $\Delta\nu$
- Surface metallicity,  $[\text{M}/\text{H}]_{\text{surf}}$
- Age,  $\tau$

We trained an artificial neural network (ANN) on the data generated by the grid of stellar models to map their fundamentals to observables. We split the grid of models into a *train* and *test* dataset for tuning the ANN, as described in Section 3.2.1. We tested a multitude of ANN configurations and training data augmentations,

evaluating them with the validation set in Section 3.2.2. We reserved a randomly generated set of stellar models as our final *validation* dataset, to evaluate the approximation ability of the ANN. In Section 3.2.3, we trained the optimal ANN on the training and test dataset and evaluated it on the validation dataset. In this section we briefly describe the theory and motivation behind the ANN.

The ANN is a network of artificial *neurons* which each transform some input vector,  $\mathbf{x}$  based on trainable *weights*,  $\mathbf{w}$  and a *bias*,  $b$  (see CITATIONS). Deep learning (DL) is the case where neurons are arranged into a series of layers such that any neuron in layer  $k - 1$  is connected to at least one of the neurons in layer  $k$ . For this work, we considered a fully-connected ANN, where each neuron in layer  $k - 1$  is connected to every neuron in layer  $k$ . The weights are represented by the connections between neurons and the bias is a unique scalar associated with each neuron. We also restricted our configuration to one with the same number of neurons,  $N$  in each hidden layer. The output of a given neuron,  $i$  in layer  $k$  is,

$$x_{i,k} = f_k(\mathbf{w}_{i,k} \cdot \mathbf{x}_{k-1} + b_{i,k}) \quad (3)$$

where  $f_k$  is the *activation* function for the  $k$ -th layer,  $\mathbf{w}_{i,k}$  are the weights connecting all the neurons in layer  $k - 1$  to the current neuron, and  $b_{i,k}$  is the bias. This generalises such that the output of the  $k$ -th layer is,

$$\mathbf{x}_k = f_k(\mathbf{W}_k \cdot \mathbf{x}_{k-1} + \mathbf{b}_k), \quad (4)$$

where  $\mathbf{W}_k$  is the matrix of weights leading to all neurons in the  $k$ -th layer. For a regression neural network, we typically have a linear activation function applied to the output of the final layer. Therefore, the output of a network of  $M$  hidden layers with initial input  $\mathbf{X}$  is,

$$\mathbf{Y} = \mathbf{W}_M \cdot f_{M-1}(\dots f_1(\mathbf{W}_1 \cdot f_0(\mathbf{W}_0 \cdot \mathbf{X} + \mathbf{b}_0) + \mathbf{b}_1)) + \mathbf{b}_M, \quad (5)$$

$$\equiv \eta_{\text{net}}(\mathbf{X}). \quad (6)$$

Hereafter, we refer to our choice of neurons per layer,  $N$  and hidden layers  $M$  as the *architecture*.

To fit the ANN, we used a set of training data,  $\mathbf{D}_{\text{train}} = \{(\mathbf{X}_1, \mathbf{Y}_1) \dots (\mathbf{X}_{N_{\text{train}}}, \mathbf{Y}_{N_{\text{train}}})\}$  comprising  $N_{\text{train}}$  input-output pairs. We split the training data into pseudo-random batches,  $\mathbf{D}_{\text{batch}}$  because this has been shown to improve model convergence (CITE)

and computational efficiency. An error function,  $E(D_{\text{batch}})$ , also known as the *loss*, quantifies the difference between the predictions and the training data. The weights are updated after each batch using an algorithm called the *optimizer* with the goal of minimising the loss. We also considered an addition to the loss called *regularisation* which helps reduce over-fitting (CITE).

We varied the architecture, number of batches, choice of loss function, optimizer and regularisation during the optimisation phase. We initialised each ANN with a random set of weights and biases and minimized the loss over a given number of *epochs*. An epoch is defined as one iteration through the training dataset,  $D$ . We tracked the loss for each ANN using an independent test dataset to determine the most effective choice of ANN parameters (see Section 3.2.2).

During initial tuning, we found that having stellar age as an input was unstable, because it varied a lot with the other input parameters. We solved this by introducing a metric to describe the fraction of time a star has spent at a given evolutionary phase,  $f_{\text{evol}}$ .

$$f_{\text{evol}} = \begin{cases} f_{\text{MS}}, & f_{\text{MS}} \leq 1 \\ 1 + \frac{\text{age} - \tau_{\text{MS}}}{\text{age}_{\log g=3.6} - \tau_{\text{MS}}}, & f_{\text{MS}} > 1 \end{cases} \quad (7)$$

where  $\text{age}_{\log g=3.6}$  is the age of the star at the end of the track,

$$f_{\text{MS}} = \frac{\text{age}}{\tau_{\text{MS}}}, \quad (8)$$

and  $\tau_{\text{MS}}$  is the star's main sequence lifetime, defined in the models as the point where the central hydrogen fraction,  $X_c < 0.XX$ . In other words, a star with  $f_{\text{evol}} \in (0, 1]$  is in its main sequence phase, burning hydrogen in its core, and  $f_{\text{evol}} \in (1, 2]$  has left the main sequence and begins burning hydrogen in a shell. By proxy, this gives the ANN information about the internal state of the star which effects the output observables. Otherwise,  $f_{\text{evol}}$  is a meaningless parameter, although it could loosely be interpreted as a measure of the evolutionary phase of the star.

We chose the ANN input and output parameters to be  $X = \{f_{\text{evol}}, M, \alpha_{\text{mlt}}, Y_{\text{init}}, Z_{\text{init}}\}$  and  $Y = \{\log(\text{age}), T_{\text{eff}}, R, \Delta\nu, [M/H]_{\text{surf}}\}$  respectively. The inputs correspond to initial conditions in the stellar modelling code and the outputs correspond to surface conditions throughout its lifetime, with the exception of age which is mapped from  $f_{\text{evol}}$ . A generalised form of the neural network is depicted in Figure 1.

### 3.2.1 Training data

Firstly, consider re-sampling the grid data weighted by position on a Kiel diagram ( $\log g$  and  $\text{teff}$ ) so that we have good coverage of observables. This will help the network train better.

Then explain normalization of the data.

Describe the train-test split as a way of optimizing the neural network architecture without being biased towards the training data. I.e. we chose parameters based on what minimises the difference between train and test loss. We reserved 20 per cent of the on-grid dataset for validation. This allowed us to assess our choice of ANN hyperparameters without being biased towards the specific set of training data.

Some histograms showing the training and test data may be useful.

We pseudo-randomly sampled 7 000 000 points from the grid of stellar models as the training dataset, with the remaining [CHECK THIS] 2 000 000 points given to the test dataset. Before we trained a given ANN architecture, we standardised the training dataset by

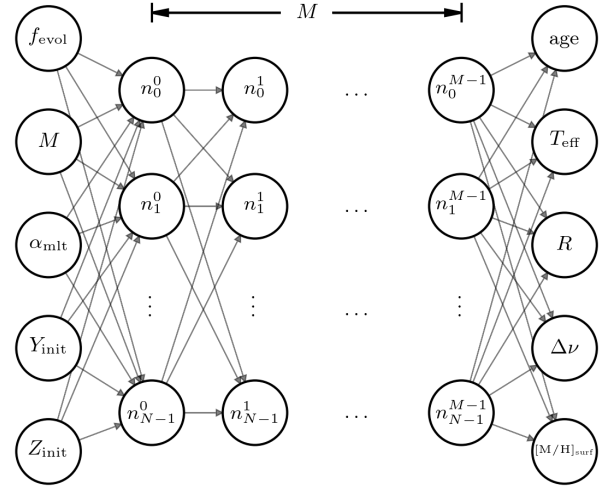


**Figure 1.** An artificial neural network comprising  $M$  hidden layers with  $N$  neurons per layer. Arrows connecting the nodes represent tunable weights.

subtracting the median and dividing by the standard deviation. We show the locations and scales of the standardisation for each parameter in Table 3.

We produced a validation dataset of [CHECK THIS] 2 000 000 off-grid stellar models with randomly generated initial conditions. This dataset was set aside and evaluated on the final ANN.

We show the training, test and validation datasets in Figure ??.

### 3.2.2 Tuning

Some description of how we went about choosing the network architecture and what we eventually settled on. A diagram showing the network architecture with explanation.

#### THIS IS A ROUGH DRAFT

A generic form of the ANN architecture is shown in Figure 1. We varied the number of neurons,  $N$  per hidden layer and the total number of hidden layers,  $M$  and the choice of activation function. We also considered the addition of regularisation of the weights, which act to add random scatter to the weights to help dislodge weights stuck in local minima. The impact of these parameters were assessed by looking at the behaviour of the train and test loss with respect to the number of epochs and wall time. The closer the test loss was to the training loss, the better.

The choice of batch size (i.e. the number of forward passes before updating the weights) was also found to impact the training. A smaller batch size helped the ANN converge faster and was less computationally expensive. The final batch size was chosen as a trade-off between GPU efficiency and convergence speed.

The final choice of architecture was  $N = 128$  neurons for each of  $M = 6$  hidden layers. We found that the exponential linear unit (ELU) was the most appropriate choice of activation function over the more popular rectified linear unit (ReLU), although ReLU would converge faster. ELU suited the smooth nature of the stellar evolutionary tracks better, whereas ReLU contains a gradient discontinuity which caused poorer sampling later-on during modelling.

The neural network was then trained on the full train-test dataset for a total of 24 hours before being evaluated using an



**Table 3.** The median,  $\mu_{1/2}$  and standard deviation,  $\sigma$  for each parameter in the training data, used to standardise the dataset.

	Input					Output				
	$f_{\text{evol}}$	$M (M_{\odot})$	$\alpha_{\text{mlt}}$	$Y_{\text{init}}$	$Z_{\text{init}}$	$\log(\text{age/Gyr})$	$T_{\text{eff}} (K)$	$R (R_{\odot})$	$\Delta\nu (\mu\text{Hz})$	$[M/H]_{\text{surf}} (\text{dex})$
$\mu_{1/2}$	0.865	1.000	1.900	0.280	0.017	0.790	5566.772	1.224	100.720	0.081
$\sigma$	0.651	0.118	0.338	0.028	0.011	0.467	601.172	0.503	42.582	0.361

independent validation dataset described in Section ???. The final training loss was a mean absolute error of XX.XX.

We tuned the ANN parameters by varying them in both a grid-based and heuristic approach.

SHOW A TABLE AND PLOT WITH AN EXAMPLE OF ARCHITECTURES AND THEIR TRAINING PERFORMANCE. EXPLAIN WHY WE OPTED FOR THE FINAL MODEL.

### 3.2.3 Validation

Here will be a summary of the neural network accuracy for the train, test and validation datasets.

We trained the final ANN for [CHECK] 50 000 epochs<sup>1</sup> where it reached a test mean absolute error of [CHECK] 0.001.

### 3.3 Probabilistic model

We devised three Bayesian models, each with varying levels of parameter sharing between stars in the sample. Initially, we tested the models and demonstrated shrinkage of statistical uncertainties in the stellar fundamental parameters by analysing a random sample of 100 stars modelled using MESA. Then, we applied the models to the sample of stars collated in Section ?? and compared the results with that of S17.

The first model is equivalent to modelling each star individually and features no parameter sharing; as such, we refer to it as the no-pooled (NP) model. We then introduce two hierarchical Bayesian models (HBMs) which employ population-level parameters to describe their distribution in the sample. Both models partially-pool helium via a linear enrichment law. In other words, the initial helium fraction for each star is drawn from a normal distribution, with a mean described by the enrichment law and standard deviation to describe the deviation of helium from said law. One model also partially-pools the mixing-length theory parameter,  $\alpha_{\text{mlt}}$  in a similar way, whereas the other maximally-pools  $\alpha_{\text{mlt}}$  such that it assumes the same value for the entire sample. We refer to the former as the max-pooled (MP) model and the latter as the partial-pooled (PP) model. All three models are described in the following subsections.

We sampled the posterior for each model using the No U-Turn Sampler (NUTS) of PyMC4 [CITE]. Initially, we modelled each star individually in order to identify stars outside the grid range and other sampling problems. We flagged stars with median modelled values outside the grid range by more than the median 16th or 84th percentile in the sample.

#### 3.3.1 No-pooled model

Firstly, we constructed a model comprising independent parameters  $\theta_i = \{f_{\text{evol},i}, M_i, \alpha_{\text{mlt},i}, Y_i, Z_i\}$  for a given star,  $i$ . Using Bayes'

theorem, the *posterior* probability density function (PDF) of the model parameters given a set of observed data,  $\mathbf{y}_i$  is,

$$p(\theta_i | \mathbf{y}_i) \propto p(\theta_i) p(\mathbf{y}_i | \theta_i), \quad (9)$$

where  $p(\theta_i)$  is the *prior* PDF of the model parameters and  $p(\mathbf{y}_i | \theta_i)$  is the *likelihood* of observing the data given the model.

We chose weakly-informative, bounded priors for the independent parameters, restricting them to their respective ranges in the ANN training data. Although the neural network is able to make predictions outside the training data range, these have not been tested and may be unreliable. Therefore, we used a beta distribution with  $\alpha = \beta = 1.2$  as the prior PDF on the independent parameters, transformed such that the probability is null outside the chosen range,

$$p(\theta_i) = \prod_{k=1}^{N_{\theta}} \left[ \theta_{k,\text{min}} + (\theta_{k,\text{max}} - \theta_{k,\text{min}}) \mathcal{B}(\theta_{k,i} | 1.2, 1.2) \right], \quad (10)$$

where the beta distribution is defined as,

$$\mathcal{B}(x | \alpha, \beta) = \frac{x^{\alpha-1} (1-x)^{\beta-1}}{\int_0^1 u^{\alpha-1} (1-u)^{\beta-1} du}. \quad (11)$$

The beta distribution was preferred over a bounded uniform distribution because our sampler evaluates the gradient of the posterior and hence sensitive to discontinuities.

We made predictions for each star using the trained ANN,  $\{\log(\text{age})_i, T_{\text{eff},i}, R_i, \Delta\nu_i, [M/H]_{\text{surf},i}\} = \eta_{\text{net}}(\theta_i)$ , from which we derived the luminosity,  $L_i$  using the Stefan-Boltzmann law. Any of the model parameters may be passed as an observable. Hereafter, we denote the set of model observables as  $\mu_{y,i} = \mu_y(\theta_i)$ . Thus, we write the likelihood we observe any  $\mathbf{y}_i$  with uncertainty,  $\sigma_y$  given the model as,

$$p(\mathbf{y}_i | \theta_i) = \prod_{k=1}^{N_{\text{obs}}} \frac{1}{\sigma_{y,k,i} \sqrt{2\pi}} \exp \left[ -\frac{(y_{k,i} - \mu_{y,k}(\theta_i))^2}{2\sigma_{y,k,i}^2} \right], \quad (12)$$

where  $N_{\text{obs}}$  is the number of observed variables. We chose to use observed  $T_{\text{eff}}$ ,  $L$ ,  $\Delta\nu$  and  $[M/H]$  collated for our sample as described in Section ??.

Using the above model, we sampled from the posterior for each individual star separately and then together as a population of  $N_{\text{stars}}$  stars,  $p(\theta | \mathbf{y}) = \prod_{i=1}^{N_{\text{stars}}} p(\theta_i | \mathbf{y}_i)$ . Separate modelling allowed us to identify poorly sampled posteriors, whether the model indicated a fit outside the given input range, or other sampling issues. Once a refined sample was chosen, modelling the sample all together was done as a natural application of the ANN through the use of batching. The ANN inputs were modelled as independent distributions, then the random variables were batched together and passed through the ANN to produce predictions for each star.

#### 3.3.2 Partial-pooled model

Sharing, or pooling parameters between stars in a population can improve the uncertainties on stellar fundamentals by encoding our prior

<sup>1</sup> This took approximately [CHECK] 48 hours on an NVidia Tesla V100 graphics processing unit.

knowledge of their distribution in a population. We constructed a hierarchical model [CITE Gelman?], which builds upon the NP model by introducing population-level *hyperparameters*. Specifically, we chose to describe initial helium and  $\alpha_{\text{mlt}}$  by partially-pooling them.

We constructed the PP model such that each of the initial helium,  $Y_{\text{init}}$  and mixing-length theory parameter,  $\alpha_{\text{mlt}}$  are drawn from a common distribution characterised by the set of hyperparameters,  $\phi = \{\Delta Y/\Delta Z, Y_P, \sigma_Y, \mu_\alpha, \sigma_\alpha\}$ . Thus, Bayes' theorem becomes,

$$p(\theta, \phi | y) \propto p(\phi) p(Y_{\text{init}}, \alpha_{\text{mlt}} | \phi) p(y | \theta), \quad (13)$$

where  $\theta$  is the same as in the NP model, each object-level parameter,  $\theta_j = \{\theta_{j,i}\}_{i=1}^{N_{\text{stars}}}$  and  $\psi = \{f_{\text{evol}}, \mathbf{M}, \mathbf{Z}\}$  are the subset of object-level parameters not governed by the hyperparameters.

We assumed the initial helium and the mixing-length parameter are drawn from a normal distribution characterised by a population mean and standard deviation,

$$p(Y_{\text{init}}, \alpha_{\text{mlt}} | \phi) = p(Y_{\text{init}} | \mu_Y, \sigma_Y) p(\alpha_{\text{mlt}} | \mu_\alpha, \sigma_\alpha). \quad (14)$$

Regarding the first term of this equation, the mean initial helium follows a linear enrichment law with respect to the initial fraction of heavy-elements for a given star,

$$\mu_Y = Y_P + \frac{\Delta Y}{\Delta Z} Z_{\text{init}}, \quad (15)$$

where  $Y_P$  is the primordial helium abundance fraction and  $\Delta Y/\Delta Z$  is the so-called enrichment ratio. Therefore, we may write the prior PDF of initial helium given its population-level hyperparameters as,

$$p(Y_{\text{init}} | Z_{\text{init}}, \Delta Y/\Delta Z, Y_P, \sigma_Y) = \prod_{i=1}^{N_{\text{stars}}} \mathcal{N}(Y_{\text{init},i} | \mu_{Y,i}, \sigma_Y) \quad (16)$$

We justified this assumption based on theoretical and empirical evidence for a linear enrichment law ( ), but taking into account an intrinsic spread,  $\sigma_Y$  about this law due to random variations in chemical abundance throughout the interstellar medium.

Similarly, for the second term of Equation 14, we chose to partially-pool the mixing-length parameter. We assume that convection in stars of a similar mass, evolutionary stage and area of the HR diagram may be approximated using a similar value of  $\alpha_{\text{mlt}}$ , but the accuracy of the mixing-length theory may vary from star-to-star. There is theoretical evidence for such a variation with  $[M/H]$ ,  $T_{\text{eff}}$  and  $\log g$  in 3D hydrodynamical stellar models (Magic et al. 2015; Viani et al. 2018). However, investigating such dependencies are beyond this scope of this paper. Given the small range of our sample, any such variation will be absorbed by the spread parameter,  $\sigma_\alpha$ . Therefore, we decided to describe the prior on  $\alpha_{\text{mlt}}$  as,

$$p(\alpha_{\text{mlt}} | \mu_\alpha, \sigma_\alpha) = \prod_{i=1}^{N_{\text{stars}}} \mathcal{N}(\alpha_{\text{mlt},i} | \mu_\alpha, \sigma_\alpha) \quad (17)$$

We gave all of the hyperparameters weakly informative priors, with the exception of  $Y_P$  for which we adopt a recent measurement of the primordial helium abundance the mean [CITE PLANK] with a standard deviation representative of the range of values in the literature [CITE]. We assumed priors on the hyperparameters as follows,

$$\begin{aligned} \Delta Y/\Delta Z &\sim 4.0 \mathcal{B}(1.2, 1.2), \\ Y_P &\sim \mathcal{N}(0.247, 0.1), \\ \sigma_Y &\sim \mathcal{LN}(0.01, 1.0), \\ \mu_\alpha &\sim 1.5 + \mathcal{B}(1.2, 1.2), \\ \sigma_\alpha &\sim \mathcal{LN}(0.1, 1.0), \end{aligned}$$

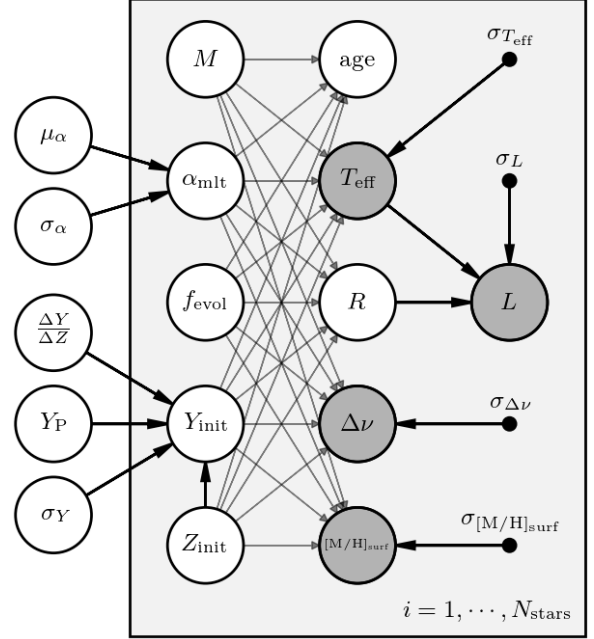


Figure 2.

where  $x \sim \mathcal{LN}(m, \sigma)$  represents a random variable drawn from the log-normal distribution,

$$\mathcal{LN}(x|m, \sigma) = \frac{1}{x\sigma\sqrt{2\pi}} \exp\left[-\frac{\ln(x/m)^2}{2\sigma^2}\right]. \quad (18)$$

### 3.3.3 Max-pooled model

We built another hierarchical model similar to the PP model except that  $\alpha_{\text{mlt}}$  is max-pooled. In other words, we assumed that the mixing length must be the same value for every star in the sample, but still allowed it to freely vary. Thus the hyperparameters are now,  $\phi = \{\Delta Y/\Delta Z, Y_P, \sigma_Y, \alpha_{\text{mlt}}\}$ . The posterior distribution of the model takes the same form as in Equation 13 except that now,

$$p(\alpha_{\text{mlt}} | \alpha_{\text{mlt}}) = \prod_{i=1}^{N_{\text{stars}}} \delta(\alpha_{\text{mlt},i} | \alpha_{\text{mlt}}) \quad (19)$$

where  $\delta(x|\alpha)$  is defined as,

$$\delta(x|\alpha) = \begin{cases} +\infty, & x = \alpha \\ 0, & x \neq \alpha \end{cases} \quad (20)$$

## 4 RESULTS

We obtained model stellar fundamental parameters for each of the NP, PP and MP models by taking the median and 68 percent credible region from the marginalised posterior samples. For the test stars, we compared the results with the true values for each of the models. We found good agreement with the true values and showed that the uncertainties on mass, age and radius decrease with increasing sample size in the PP model. We also found that the NP method over-predicts the uncertainties on the fundamental parameters due to poorly sampling  $Y_{\text{init}}$  and  $\alpha_{\text{mlt}}$ . Fitting the helium enrichment law

and spread in mixing-length to the NP model results recovered the true hyperparameters with higher precision than the PP and MP models. However, fitting this way limited the precision of the stellar parameters, whereas the hierarchical models reduced the uncertainties by roughly a factor of  $\sqrt{N_{\text{stars}}}$ . The results for the test stars are shown in more detail in Appendix ??.

With confidence that the models were able to obtain accurate stellar parameters, in accordance with our choice of stellar models, we present results for the sample of 81 *Kepler* dwarfs for each of our statistical models. Tables of results for each model are available for download at [TODO](#).

We obtained results for the hyperparameters in each of the models and present them in Table 4. For NP, we fit the same hyperparameters from the PP model to the results from the NP model, using the same prior distributions.

The PP and MP results without the Sun are self-consistent, but the biggest difference between the two methods is evident when the Sun is added. The MP model will typically settle for a shared value of  $\alpha_{\text{mlt}}$  which favours the star with the best observational constraints. In our case, the solar model yields  $\alpha_{\text{mlt}} = 2.11^{+0.01}_{-0.01}$  which is far from  $\alpha_{\text{mlt}}$  of  $1.73^{+0.08}_{-0.07}$  obtained without the Sun. However, when  $\alpha_{\text{mlt}}$  is partially-pooled, the  $\sigma_{\alpha}$  parameter copes with this by increasing to include the Sun in the distribution. The PP models are more robust.

We noticed that the uncertainties on the NP hyperparameters were smaller than those of the hierarchical models. However, these are likely underestimated because the NP model poorly constrains  $\alpha_{\text{mlt}}$  and  $Y_{\text{init}}$  such that the bounds of the prior have the effect of reducing the standard deviation of their marginalized posteriors. On the contrary, the hierarchical models [SOMETHING...](#)

We found that including the sun in our PP and MP models systematically shifted the median ages of the sample by about 0.5 Gyr and 1.0 Gyr respectively (Figure ??). This is a direct result of the solar model favouring a higher  $\alpha_{\text{mlt}}$  and lower  $Y_{\text{init}}$  than the rest of the sample. Partially pooling the sun with the rest of the sample copes with this better by accounting for a population spread in the parameters, hence the smaller difference with and without the Sun.

## 5 DISCUSSION

We have shown that, utilising hierarchical models, it is possible to reduce the statistical uncertainties on fundamental stellar parameters by sharing information between the stars. However, as such uncertainties reduce, systematics begin to dominate. We stress that the next challenge is to robustly model the systematic uncertainties between stellar modelling codes and within observables. Until then, we hesitate to publish one preferred set of parameters for our sample of stars. Instead, this paper is a demonstration of our method.

## 6 CONCLUSIONS

### ACKNOWLEDGEMENTS

### REFERENCES

- Asplund M., Grevesse N., Sauval A. J., Scott P., 2009, [ARA&A](#), 47, 481  
 Ferguson J. W., Alexander D. R., Allard F., Barman T., Bodnarik J. G., Hauschildt P. H., Heffner-Wong A., Tamanai A., 2005, [The Astrophysical Journal](#), 623, 585  
 Huber D., et al., 2011, [ApJ](#), 743, 143  
 Magic Z., Weiss A., Asplund M., 2015, [A&A](#), 573, A89  
 Paxton B., Bildsten L., Dotter A., Herwig F., Lesaffre P., Timmes F., 2011, [ApJS](#), 192, 3

- Paxton B., et al., 2013, [The Astrophysical Journal Supplement Series](#), 208, 4  
 Paxton B., et al., 2015, [The Astrophysical Journal Supplement Series](#), 220, 15  
 Paxton B., et al., 2018, [The Astrophysical Journal Supplement Series](#), 234, 34  
 Paxton B., et al., 2019, [The Astrophysical Journal Supplement Series](#), 243, 10  
 Rogers F. J., Nayfonov A., 2002, [The Astrophysical Journal](#), 576, 1064  
 Serenelli A., et al., 2017, [ApJS](#), 233, 23  
 Townsend R. H. D., Teitler S. A., 2013, [Monthly Notices of the Royal Astronomical Society](#), 435, 3406  
 Viani L. S., Basu S., Ong J. M. J., Bonaca A., Chaplin W. J., 2018, [The Astrophysical Journal](#), 858, 28  
 White T. R., Bedding T. R., Stello D., Christensen-Dalsgaard J., Huber D., Kjeldsen H., 2011, [The Astrophysical Journal](#), 743, 161  
 Zinn J. C., Pinsonneault M. H., Huber D., Stello D., Stassun K., Serenelli A., 2019, [ApJ](#), 885, 166

## APPENDIX A: TESTING THE METHOD

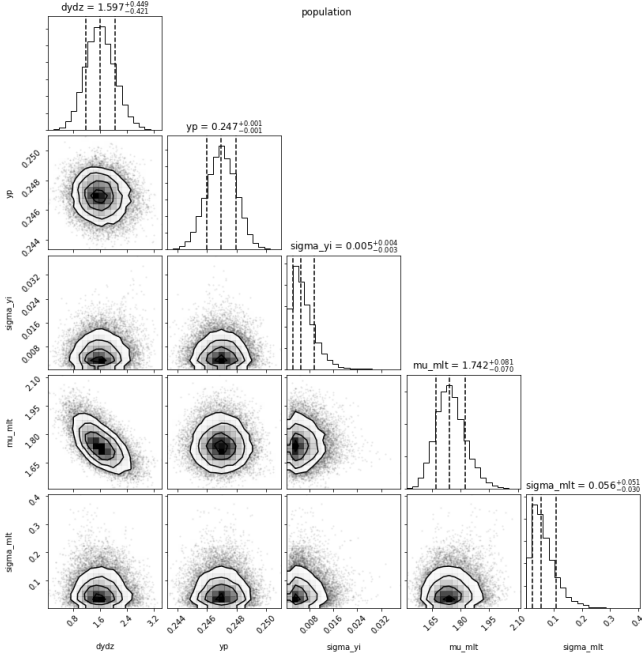
We tested the ability of the method to recover stellar fundamental properties in accordance with our choice of stellar evolution code and physics.

This paper has been typeset from a  $\text{\LaTeX}$  file prepared by the author.

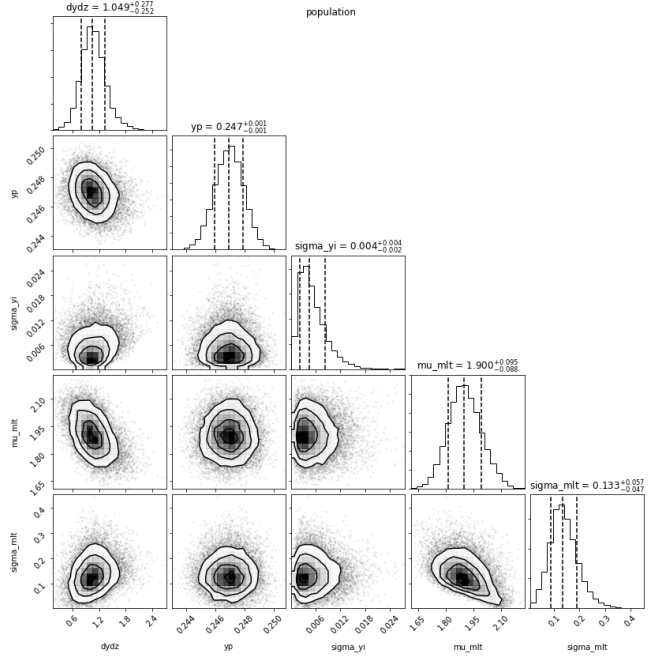


**Table 4.** Hyperparameter results for each model in descending order of the helium enrichment ratio,  $\Delta Y/\Delta Z$ .

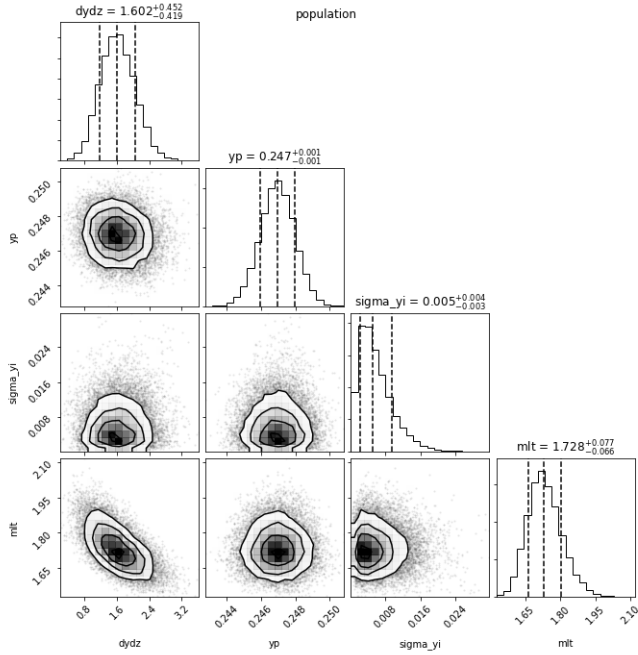
Model	$\Delta Y/\Delta Z$	$Y_P$	$\sigma_Y$	$\mu_\alpha$	$\sigma_\alpha$	$\alpha_{\text{mlt}}$
NP	$1.69^{+0.21}_{-0.21}$	$0.247^{+0.001}_{-0.001}$	$0.0074^{+0.0026}_{-0.0022}$	$1.95^{+0.04}_{-0.04}$	$0.06^{+0.03}_{-0.02}$	—
MP	$1.60^{+0.45}_{-0.42}$	$0.247^{+0.001}_{-0.001}$	$0.0051^{+0.0044}_{-0.0027}$	—	—	$1.73^{+0.08}_{-0.07}$
PP	$1.60^{+0.45}_{-0.42}$	$0.247^{+0.001}_{-0.001}$	$0.0051^{+0.0045}_{-0.0027}$	$1.74^{+0.08}_{-0.07}$	$0.06^{+0.05}_{-0.03}$	—
PPS	$1.05^{+0.28}_{-0.25}$	$0.247^{+0.001}_{-0.001}$	$0.0045^{+0.0038}_{-0.0023}$	$1.90^{+0.09}_{-0.09}$	$0.13^{+0.06}_{-0.05}$	—
MPS	$0.76^{+0.24}_{-0.27}$	$0.247^{+0.001}_{-0.001}$	$0.0049^{+0.0039}_{-0.0025}$	—	—	$2.09^{+0.03}_{-0.03}$



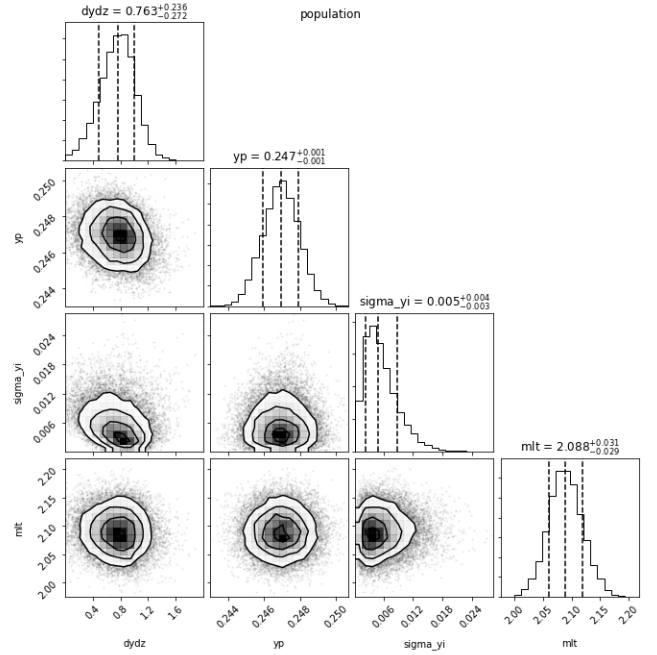
(a) Population hyperparameters for model without the Sun.



(b) Population hyperparameters for model with the Sun.

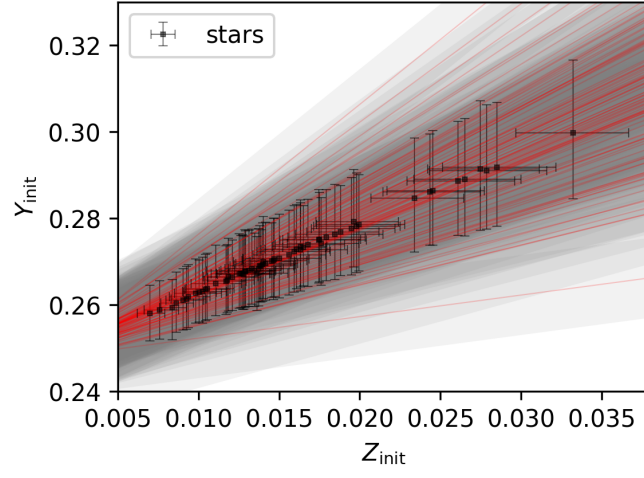


(c) Population hyperparameters for model without the Sun.

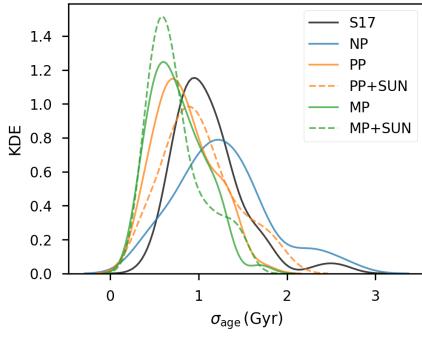


(d) Population hyperparameters for model with the Sun.

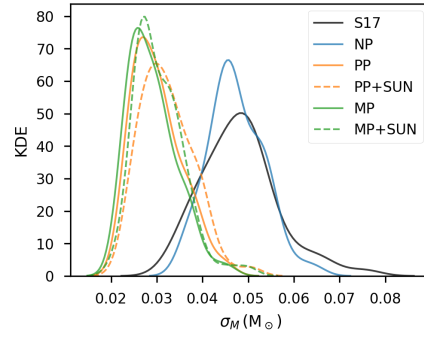
**Figure 3.**



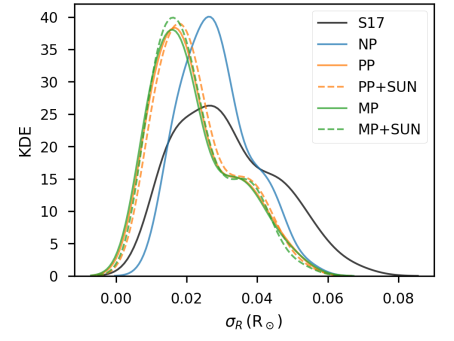
(a)



(a) Age



(b) Mass



(c) Radius

**Figure 5.** Kernel density estimates (KDEs) of the uncertainties in the results from each model compared with that of (S17).